ACS Sustainable Chemistry & Engineering

pubs.acs.org/journal/ascecg

Research Article

# Nanoscale Solid Superacid-Coupled Polybenzimidazole Membrane with High Ion Selectivity for Flow Batteries

Lei Hu,[⊥] Yue Du,[⊥] Li Gao, Mengting Di, Ning Zhang, Yu Pan, Xiaoming Yan,* Baigang An,* and Gaohong He*

Cite This: https://dx.doi.org/10.1021/acssuschemeng.0c05359

Read Online

ACCESS | Metrics & More | Article Recommendations

**ABSTRACT:** Nanoscale solid superacid $SO_4^{2-}/ZrO_2/WO_3$ is coupled into imidazole-hydroxyl-quaternary ammonium co-functionalized polybenzimidazole (PG112) to address the trade-off effect of membrane for large-scale flow battery application. Nanoscale $SO_4^{2-}/ZrO_2/WO_3$ particles with high sulfonic groups are dispersed in membrane as redox-active ion barriers and proton carriers, which mitigate the electrolyte crossover and maintain high ion conductivity. The $VO^{2+}$ permeability of the prepared membrane ($7.86 \times 10^{-10}$ cm$^2$ s$^{-1}$) is significantly lower than those of PG112 ($3.93 \times 10^{-9}$ cm$^2$ s$^{-1}$) and Nafion 212 ($7.76 \times 10^{-8}$ cm$^2$ s$^{-1}$) membranes. The vanadium flow battery with this membrane exhibits a longer self-discharge duration time of 231 h compared with Nafion 212 (35 h) and PG112 (88 h) membranes. High coulombic efficiencies of 97.5−99.2% at 40−120 mA cm$^{-2}$ are obtained for the prepared membrane, which are higher than those for Nafion 212 (78.0−92.8%) and PG112 membranes (96.2−98.6%). Stable cycle performance and low retention capacity are also observed, suggesting the excellent chemical stability of the prepared membrane in vanadium flow battery operation. This work provides a prospective and applicable membrane to enhance the performance of flow battery.

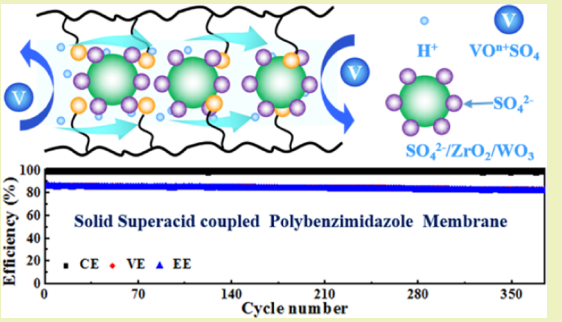


**KEYWORDS:** *nanoscale solid superacid, ion selectivity, polybenzimidazole, membrane, flow battery*

## INTRODUCTION

Energy storage systems are urgently required to address energy shortages and environmental concerns in industrial applications.[1−3] In various kinds of energy storage technologies, vanadium flow battery (VFB) has huge potential in large-scale energy storage applications due to its long life, flexibility, and safety.[4−7] As one of the core components of VFB, membrane plays a key role in selectively transporting nonreaction ions.[8−10] Commercialized membranes, such as Nafion 212 and Nafion 115, are widely employed in VFB owing to their high ion conductivity and excellent stability.[11−14] However, high electrolyte crossover and expensive price hinder their applications in VFB.[11,15] Therefore, the critical issue of VFB is to design alternative membranes with the properties of low cost, high ion-selective conductivity, and long-term stability.[16−20]

Much effort has been made to develop advanced membranes, such as functionalized polysulfone (PSF),[21−23] poly(ether ether ketone) (PEEK),[24−28] poly(vinylidene fluoride) (PVDF),[29,30] polyimide,[31−33] and polybenzimidazole (PBI).[34−37] Among these potential alternatives, PBI-based membranes show outstanding chemical stability and excellent ion selectivity.[38−41] The high area resistance of dense PBI membrane causes a large voltage efficiency (VE) loss at high current densities due to the serious Ohmic polarization.[42] The porous structures constructed by the phase inversion method could enhance ion conductivity.[34,43−45] However, the formation of a precise pore structure is still an important challenge. The assemblies of sulfonic acid groups, amino groups, polyether groups, or hydroxyl groups could promote the formation of nanophase separated structure; thus, successive ion-transport channels are formed to increase the ion conductivity of the PBI membrane.[46−49] In our previous work,[50] the imidazole-hydroxyl-quaternary ammonium co-functionalized PBI was proposed to achieve a high performance of VFB based on the synergistic effect of three functional groups. PBI anion-exchange membrane with highly co-functionalized degree had wide ion-transport channels for high VE, which was accompanied with high electrolyte crossover, resulting in a low coulombic efficiency (CE) in VFB operation. Although a high EE was accomplished due to

Received: July 21, 2020
Revised: September 20, 2020

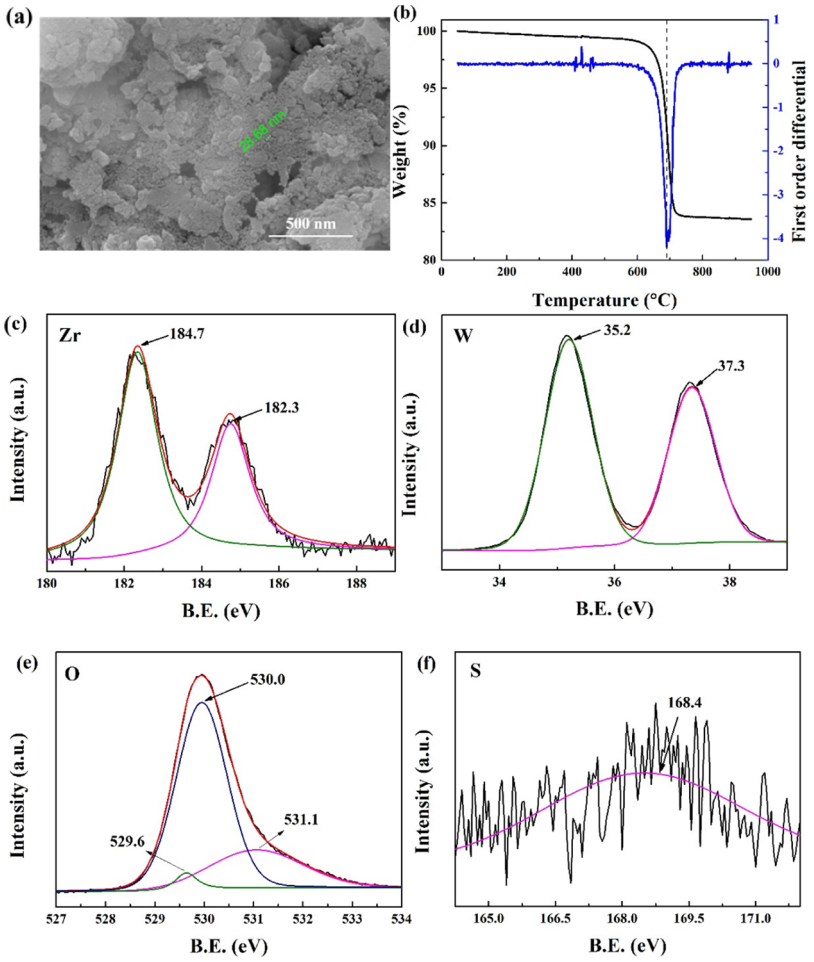


**Figure 1.** Morphology and structure of $SZW_{0.4}$ nanoparticles: (a) SEM image; (b) TGA curve; (c) Zr 3d; (d) W 4f; (e) O 1s; and (f) S 2p.

the significantly enhanced VE, the CE suffered a decline due to the low selectivity of the wide ion-transport channels.

Incorporating nanoparticles into a polymer matrix could improve the ion selectivity of membrane.[35,51,52] Qiu and co-workers fabricated a sulfonated PEEK/graphene oxide nanocomposite membrane with low redox-active ion permeability and high ion selectivity, which displayed a stable CE of ~99% over 1200 cycles as well as low capacity fading.[53] Meng and co-workers modified a Nafion membrane with silica-containing phosphotungstic acid, which exhibited a 6.8 times higher ion selectivity than Nafion.[54] Shi and co-workers introduced graphitic carbon nitride nanosheets into sulfonated PSF, which showed a higher ion selectivity than Nafion 117 and pristine sulfonated PSF membrane.[22] Nanofillers are usually modified by amino or/and sulfonic acid groups to enhance the dispersion of particles and avoid the reduction of ion conductivity of membrane.[28] However, further improvement of the proton conductivity of nanocomposite membranes is still necessary in VFB application.

Solid superacids have strong acidic ability, which can act as charge carriers to enhance the mobility of proton.[55,56] Herein, solid superacid $SO_4^{2-}/ZrO_2/WO_3$ coupled with imidazole-hydroxyl-quaternary ammonium co-functional polybenzimidazole (PG112) membrane is proposed for the first time to improve ion selectivity. Nanoscale fillers are uniformly dispersed in the membrane, which act as redox-active ion barriers to reduce the hydrophilic channels and thus minimize vanadium-ion permeation. Meanwhile, the sulfonic groups on the surface of the $SO_4^{2-}/ZrO_2/WO_3$ nanoparticles could interact with the imidazole-hydroxyl-quaternary ammonium groups of PG112 to form an amphoteric hydrogen-bond network, which promotes proton transport and further improve ion selectivity. The structure−function relationships between the microstructure of the membrane and their cell performance are analyzed.

## EXPERIMENTAL SECTION

**Materials.** The imidazole-hydroxyl-quaternary ammonium co-functional polybenzimidazole (PBI-GTA-112%, briefly PG112) was synthesized according to our previous work.[50] Tungstic acid ($H_2WO_4$, 99%) and zirconium diperchlorate oxide octahydrate ($ZrOCl_2{\cdot}8H_2O$, 98%) were purchased from Shanghai Aladdin Biochemical Technology Co., Ltd. Poly(ethylene glycol) (PEG 400, LR) and dimethyl sulfoxide (DMSO, AR) were commercially obtained Damao Chemical Reagent Factory. Ethanol (AR) and acetone (AR) were commercially obtained from TianJin FUYU Fine Chemical and used without further purification.

**Preparation of Solid Superacid $SO_4^{2-}/ZrO_2/WO_3$.** The synthesis of solid superacid $SO_4^{2-}/ZrO_2/WO_3$ has been described previously.[57] Ethanol/deionized water mixture (30 mL) with a volume ratio of 5:1 was added into a 50 mL flask. Then, 1.9 g of $ZrOCl_2{\cdot}8H_2O$ was added. After complete dissolution, 2 mL of PEG was added to the solution and then the mixture was kept at 75 °C for 4 h. Subsequently, 1 M NaOH was added slowly until pH was in the range of 9−10. Then, the formed gelatinous mixture was aged for 1 day. The resulted gelatinous product was rinsed with ethanol before


https://dx.doi.org/10.1021/acssuschemeng.0c05359
ACS Sustainable Chem. Eng. XXXX, XXX, XXX−XXX

treating in an oven at 110 °C for 4 h. The resulted white solid powders (1 g) and different masses of $H_2WO_4$ powders were immersed in 1 M $H_2SO_4$ solution for 6 h together and then treated in an oven at 110 °C for 4 h. The solid superacids $SO_4^{2-}/ZrO_2/WO_3$ (SZW) were obtained after treating in a muffle at 550 °C for 6 h. The SZW with different mass ratios of $H_2WO_4$ to $ZrO_2$ were denoted as $SZW_x$, where $x$ changed from 0.2: 1, 0.4: 1, to 0.6: 1, denoted as $SZW_{0.2}$, $SZW_{0.4}$, and $SZW_{0.6}$, respectively.

**Membrane Preparation.** The $SZW_x$ powders were ultrasonically dispersed in 5 mL of DMSO over 6 h, and then a PG112 matrix was added and completely dissolved in the solution under vigorous stirring. Next, the mixture was cast on a 5 cm × 5 cm glass plate and then dried in an oven at 60 °C for 36 h. A series of PG112-$SZW_x$-$X$ membranes were obtained by controlling the mass of $SZW_x$, where $X$ indicates the mass ratio of SZW to PG112, whose values were 0.5, 1, 1.5, and 2 wt %, respectively. The thickness of the PG112-$SZW_x$-$X$ membranes was ∼30 $\mu$m.

**Structural and Morphology Characterizations.** FT-IR spectra of the PG112-$SZW_x$-$X$ samples were recorded on a Thermo Scientific Nexus 670 FT-IR spectrophotometer. The morphologies of the membranes were tested by a scanning electron microscope (SEM, Nova NanoSEM 450). A thermogravimetric analyzer (Mettler Toledo TGA/SDTA851e) was adopted to obtain TGA curves of $SZW_x$. The thermal stability test was conducted in the temperature range of 50−800 °C with a 10 °C $min^{-1}$ heating rate in a nitrogen environment. X-ray photoelectron spectroscopy (XPS) spectra were recorded on an ESCALAB 250Xi spectrometer (Thermo Fisher). Gas adsorption and desorption analyses were done with an automatic physical adsorption instrument (Autosorb-iQ-C).

**Property Measurements.** The ion-exchange capacity (IEC) of the sample was measured by the titration method. Water uptake (WU) and swelling ratio (SR) of the membrane were measured in 3 M $H_2SO_4$ solution. Area resistance (AR) of the membrane was determined in 3 M $H_2SO_4$. The $VO^{2+}$ permeability of the sample was determined according to our previous work.[47]

**Battery Test.** A membrane with an effective area of 9 $cm^2$ was clamped between two half-cells consisted of carbon felt electrode and graphite felt. The carbon felt electrode (Gansu Hongwei Carbon Ltd., China) had a nominal thickness of 5 mm, which was oxidized in an air atmosphere at 400 °C for 6 h to improve electrochemical activity and hydrophilicity. $VO_2^+/VO^{2+}$ (50 mL, 1.5 M) in 3 M $H_2SO_4$ at the positive side and $V^{3+}/V^{2+}$ (50 mL, 1.5 M) in 3 M $H_2SO_4$ at the negative side were pumped for redox reaction. The battery performances were investigated at 40−120 mA $cm^{-2}$ with LANHE CT2001A, and the cutoff voltages were set in the range of 1.00−1.55 V for flow battery. The cycling test was measured at 120 mA $cm^{-2}$, and the self-discharge duration time was detected at 50% state of charge.

## RESULTS AND DISCUSSION

**Effect of SZW Content on PG112 Membrane.** *Structural and Morphology Characterization.* The size of $SZW_{0.4}$ is ∼30 nm, as analyzed by SEM (Figure 1a). Figure 1b illustrates TGA analysis, which was employed for characterizing the thermal stability of the synthesized $SZW_{0.4}$ nanoparticles. It reveals that there are two steps of $SZW_{0.4}$ nanoparticle weight loss. In the first step from 50 to 600 °C, the physical water molecules and free sulfate radicals adsorbed in the hydrated $SZW_{0.4}$ nanoparticles were removed with a percent weight loss of 1%. In the second step from 600 to 900 °C, the sulfate radical on the surface of the $SZW_{0.4}$ decomposes rapidly.[58] Based on these, $SZW_{0.4}$ exhibits enough thermal stability and can fulfill the needs in flow batteries. The XPS analysis of $SZW_{0.4}$ is presented in Figure 1c−f. The binding energies of Zr $3d^{5/2}$ and $3d^{3/2}$ are 182.3 and 184.7, respectively, which are in agreement with the values reported in the literature (Figure 1c).[59] The binding energies of W $4f^{7/2}$ and $4f^{5/2}$ are 37.3 and 35.2, respectively, which are in agreement with the characteristic peaks of $W^{6+}$ (Figure 1d).[60] The binding energies of O 1s are 529.6, 530.0, and 531.1, which originated from the lattice oxygens of $ZrO_2$ and $WO_3$, and the oxygen of the adsorbed sulfate radical on the surface of $SZW_{0.4}$ (Figure 1e). The binding energy of S 2p is 168.4, which is in agreement with the characteristic peak of $S^{6+}$, indicating the existence of sulfate radical on the surface of the $SZW_{0.4}$ (Figure 1f). These results indicate that the $SZW_{0.4}$ nanoparticle is successfully prepared.

The FTIR spectra of $SZW_x$, PG112, and PG112-$SZW_x$-$X$ membranes are shown in Figure 2. The characteristic

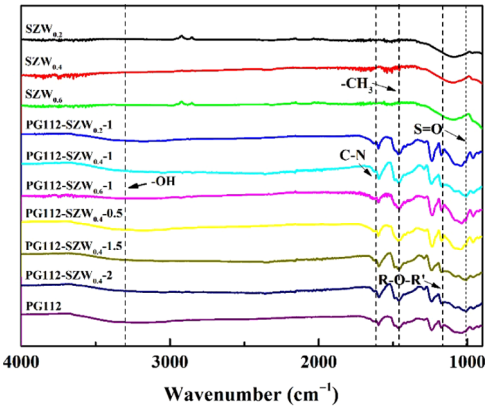


**Figure 2.** FTIR spectra of $SZW_x$, PG112, and PG112-$SZW_x$-$X$ membranes.

absorptions of S═O of $SZW_x$ are in the range of 900−1400 $cm^{-1}$ as similar to S═O of organic sulfonate, which indicate that $SZW_x$ is successfully formed. The characteristic absorptions at 1630 and 1167 $cm^{-1}$ are associated with the stretching vibration of the C═N and R−O−R′ of the PG112 polymer backbone.[48] The bands at 1460 and 3300 $cm^{-1}$ correspond to the stretching vibration of $-CH_3$ and −OH in PG112.[50] After adding $SZW_x$, a new characteristic peak at 1010 $cm^{-1}$ could be observed owing to the vibration of the S═O group, which confirm that the $SZW_x$ is successfully dispersed in the PG112 membrane.

The SEM images of the PG112 and PG112-$SZW_{0.4}$-$X$ membranes are shown in Figure 3. A defect-free morphology for dense membrane is important because defects in membrane might cause redox-active ion crossover and reduce the battery performance. It could be seen that the surfaces of PG112-$SZW_{0.4}$-$X$ membranes are dense and $SZW_{0.4}$ nanofillers are uniformly dispersed in PG112 membranes without visible aggregation phenomenon (Figure 3a−e). The observed $SZW_{0.4}$ nanofillers are also uniformly distributed in the cross sections, demonstrating excellent compatibility between PG112 and $SZW_{0.4}$ (Figure 3a′−e′ and a″−e″). This indicates that the $SZW_{0.4}$ nanofiller particles are successfully dispersed throughout the polymeric matrix and the prepared membranes are homogeneous.

The porous properties of $SZW_{0.4}$ and PG112-$SZW_{0.4}$-1 are obtained by $N_2$ desorption analysis (Figure 4a,b). The desorption isotherm reflects the typical microporous nature with a steep desorption course at a low $P/P_0$ followed by a flat course. From the results of $N_2$ desorption analysis, the pore volume and Brunauer−Emmet−Teller (BET) surface area of $SZW_{0.4}$ and PG112-$SZW_{0.4}$-1 are very small, which indicate


https://dx.doi.org/10.1021/acssuschemeng.0c05359
ACS Sustainable Chem. Eng. XXXX, XXX, XXX−XXX

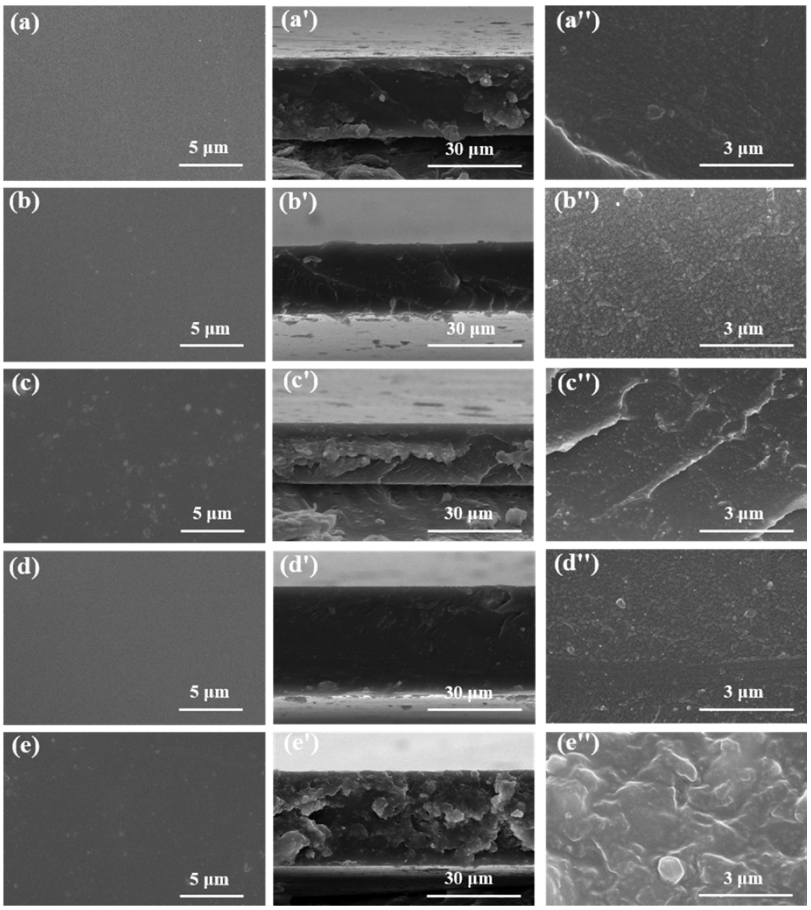


**Figure 3.** Surface images of SEM: (a) PG112, (b) PG112-$SZW_{0.4}$-0.5, (c) PG112-$SZW_{0.4}$-1, (d) PG112-$SZW_{0.4}$-1.5, and (e) PG112-$SZW_{0.4}$-2 membranes; cross-sectional images of SEM: (a′) PG112, (b′) PG112-$SZW_{0.4}$-0.5, (c′) PG112-$SZW_{0.4}$-1, (d′) PG112-$SZW_{0.4}$-1.5, and (e′) PG112-$SZW_{0.4}$-2 membranes; enlarged cross-sectional images of SEM: (a″) PG112, (b″) PG112-$SZW_{0.4}$-0.5, (c″) PG112-$SZW_{0.4}$-1, (d″) PG112-$SZW_{0.4}$-1.5, and (e″) PG112-$SZW_{0.4}$-2 membranes.

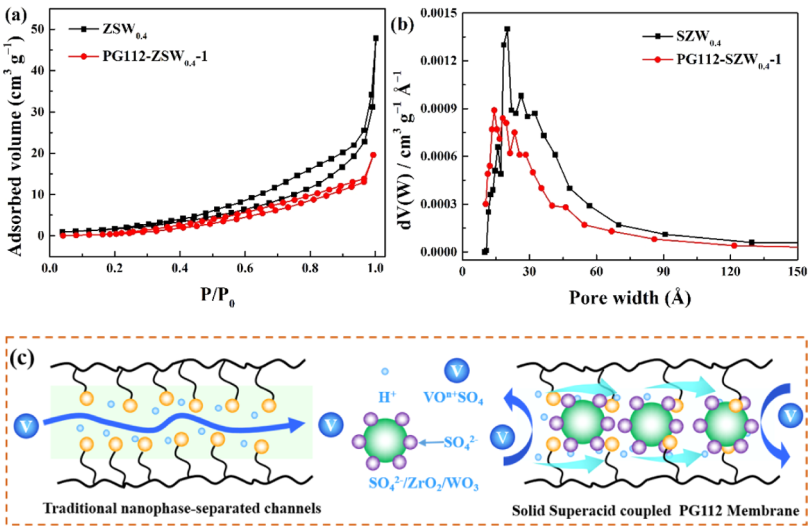


**Figure 4.** (a) $N_2$ adsorption−desorption isotherms of $SZW_{0.4}$ and PG112-$SZW_{0.4}$-1 membrane; (b) Horvath−Kawazoe pore size distribution of $SZW_{0.4}$ and PG112-$SZW_{0.4}$-1 membrane; and (c) schematic for the ion-selective transport mechanisms in nanoscale solid superacid-coupled polybenzimidazole membrane.

that $SZW_{0.4}$ has no porous structure and prepared membrane is dense and homogeneous. Based on the performance and structure described above, the nanoscale SZW are uniformly dispersed in membrane, which act as a redox-active ion barrier to reduce the hydrophilic channels and thus minimize the vanadium-ion permeation (Figure 4c). Meanwhile, the sulfonic groups of SZW could interact with the imidazole-hydroxyl-quaternary ammonium groups of PG112 to form an


https://dx.doi.org/10.1021/acssuschemeng.0c05359
ACS Sustainable Chem. Eng. XXXX, XXX, XXX−XXX

amphoteric hydrogen-bond network, which promote proton transport and further improve ion selectivity of membrane. Therefore, the prepared membrane is expected to achieve high VFB performance.

*Membrane Properties Characterization.* The performances of samples are summarized in Table 1. High WU is of benefit to proton transport. However, excess WU normally causes ineffective mechanical stability and high vanadium-ion permeability. The adsorbed water is mainly located surrounding the hydrophilic groups of PG112 chains, whereas the SZW fillers made a negligible contribution to the total water uptake. Therefore, the PG112-SZW$_x$-*X* membranes exhibited lower water uptake than the PG112 membrane, and it decreased further with the SZW content owing to the reduction of the PG112 mass percentage per unit weight. The performances of the prepared membranes with different SZW$_x$ at the same concentration were investigated. The PG112-SZW$_x$-1 membrane showed similar SR. The WU of the PG112-SZW$_{0.4}$-1 membrane is higher than those of PG112-SZW$_{0.2}$-1 and PG112-SZW$_{0.6}$-1 membranes, which could be attributed to the stronger acidic ability of SZW$_{0.4}$. The PG112-SZW$_{0.4}$-1 membranes have higher proton conductivity compared to other membranes. The PG112-SZW$_{0.4}$-*X* membranes were selected to investigate the effect of SZW contents on the performance. The WU values of the prepared membranes decrease from 30% for the PG112 membrane to 25% for the PG112-SZW-2 membrane with the increment of SZW content owing to the hydrogen-bond interaction between the sulfonic groups of SZW and the imidazole-hydroxyl-quaternary ammonium groups of PG112. At a high SZW content, the strong interaction would further decrease the size of hydrophilic channels, which would restrain the WU of the prepared membrane. The reduced WU of the membranes leads to the decrease of SR, which is beneficial to the stability and vanadium penetration resistance of the membranes. The SR decreases from 19% for the PG112 membrane to 15% for the PG112-SZW$_{0.4}$-2 membrane. It could be noted that the doped SZW has a slight effect on the proton conductivity of the PG112-SZW-*X* membranes, which is attributed to the strong acidic ability of SZW. The PG112-SZW$_{0.4}$-1.5 membrane has a higher proton conductivity compared to the PG93 membrane at the same SR and WU.[50] These results show that the prepared membrane has both high ion selectivity and ion conductivity.

**Table 1. Conductivity, SR, and WU of PG112, PG93, PG112-SZW$_x$-*X*, and PBI Membranes**

| membranes | conductivity[a] (mS cm$^{-1}$) | SR (%) | WU (%) |
|---|---|---|---|
| PG112 | 9.68 | 19 | 30 |
| PG93 | 7.90 | 15 | 26 |
| PG112-SZW$_{0.2}$-1 | 8.19 | 15 | 25 |
| PG112-SZW$_{0.4}$-1 | 9.38 | 16 | 28 |
| PG112-SZW$_{0.6}$-1 | 8.84 | 15 | 26 |
| PG112-SZW$_{0.4}$-0.5 | 9.54 | 18 | 29 |
| PG112-SZW$_{0.4}$-1.5 | 8.82 | 15 | 26 |
| PG112-SZW$_{0.4}$-2 | 7.69 | 14 | 25 |
| PBI | | 7 | 18 |

[a]Conductivity is calculated by AR.[50]

The AR of the sample in 3 M $H_2SO_4$ is shown in Figure 5a. The AR of the PG112-SZW$_{0.4}$-1 membrane is obviously lower than those of the PG112-SZW$_{0.2}$-1 and PG112-SZW$_{0.6}$-1 membranes, which mainly originated from the stronger acidic ability of SZW$_{0.4}$. On increasing the content of SZW, the AR of the PG112-SZW$_x$-*X* membranes increase slightly from 0.31 Ω cm$^2$ for the PG112 membrane to 0.38 Ω cm$^2$ for the PG112-SZW$_{0.4}$-2 membrane, which could be comparable to that of PG93 (0.38 Ω cm$^2$).[50] The low AR of a membrane means the high discharge voltage and high-operated current density of the cell. However, the conduction of protons always accompanies with the conduction of redox-active ions in the electrolytes, which would reduce the cell capacity, open-circuit voltage, and discharge voltage. The self-discharge rate and capacity fading of VFB performance depend on the redox-active ion crossover. The $VO^{2+}$ permeabilities were used to characterize the ion selectivity of membranes for VFB application (Figure 5b). Compared to the PG112 membrane, the $VO^{2+}$ permeabilities of the apll PG112-SZW$_x$-*X* membranes obviously decreased. The PG112-SZW$_x$-1 membrane showed similar $VO^{2+}$ permeabilities. For instance, the vanadium permeability of PG112-SZW$_{0.4}$-1 ($7.86 \times 10^{-10}$ cm$^2$ s$^{-1}$) is much lower than those of Nafion 212 ($7.76 \times 10^{-8}$ cm$^2$ s$^{-1}$), PG112 ($3.93 \times 10^{-9}$ cm$^2$ s$^{-1}$), and PG93 ($3.15 \times 10^{-9}$ cm$^2$ s$^{-1}$). This demonstrates that the addition of SZW nanofillers as a redox-active ion barrier reduces the hydrophilic channels and blocks the penetration of vanadium ions effectively. Consequently, owing to high ion conductivity and low $VO^{2+}$ permeability, the PG112-SZW$_{0.4}$-1 membrane can exhibit higher ion selectivity than the PG112 membrane, which results in higher performance for VFB application.

**Single-Cell Performances.** Considering the excellent balance of ion selectivity and ion conductivity, the prepared membranes are expected to achieve outstanding performances in VFB operation. The battery performances of all of the membranes at 40−120 mA cm$^{-2}$ are illustrated in Figure 6.

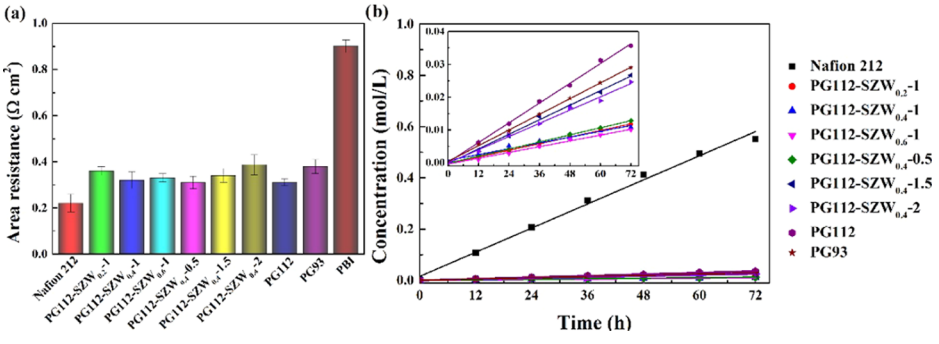


**Figure 5.** (a) AR and (b) $VO^{2+}$ permeability of PG112, PG93, PG112-SZW$_x$-*X*, and Nafion 212 membranes.


https://dx.doi.org/10.1021/acssuschemeng.0c05359
ACS Sustainable Chem. Eng. XXXX, XXX, XXX−XXX

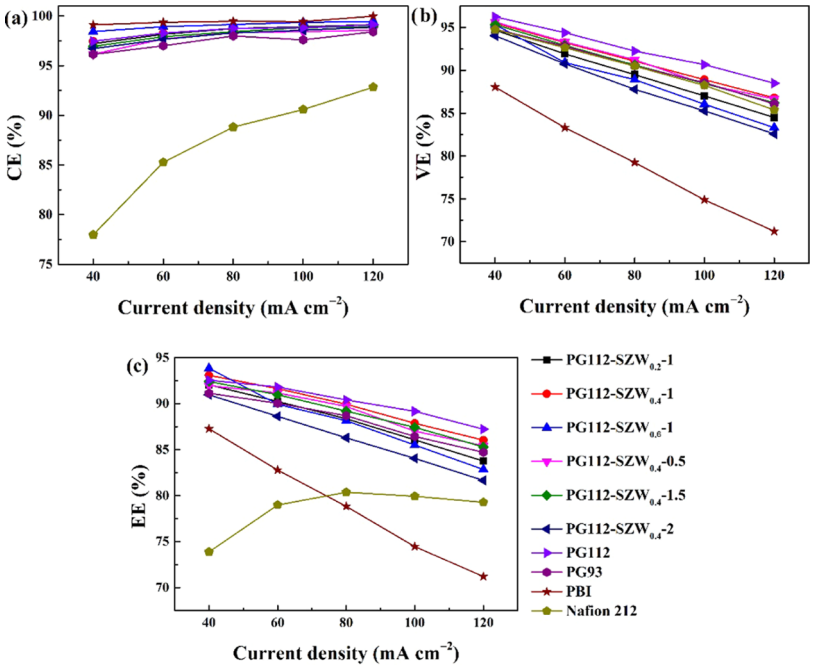


**Figure 6.** (a) CE, (b) VE, and (c) EE of battery performances with PG112, PG93, PG112-SZW$_x$-*X*, and Nafion 212 membranes at 40−120 mA cm$^{-2}$.

**Table 2. Comparison of VFB Performance with PG112-SZW$_{0.4}$-1 Membrane and Reported Membranes in Recent Years**

| | 40 mA cm$^{-2}$ | | | 80 mA cm$^{-2}$ | | | 120 mA cm$^{-2}$ | | | |
|---|---|---|---|---|---|---|---|---|---|---|
| membrane | CE | VE | EE | CE | VE | EE | CE | VE | EE | refs |
| PG112-SZW$_{0.4}$-1 | 97.5 | 95.5 | 93.1 | 98.8 | 91.1 | 89.9 | 99.1 | 86.8 | 86.0 | this work |
| SPBI-30 | 98.3 | 92.1 | 90.6 | 99.9 | 85.1 | 85.1 | 99.5 | 79.0 | 78.6 | 49 |
| *p*-TPN1 | 98.6 | 92.8 | 91.5 | 99.4 | 86.5 | 86.0 | | | | 61 |
| MD$_{2.0\text{-}10}$ | 96.2 | 91.2 | 87.7 | 99.1 | 82.8 | 82.0 | | | | 62 |
| PVDF | 88.8 | 91.7 | 81.4 | 93.7 | 84.2 | 78.9 | 95.3 | 76.7 | 73.2 | 30 |
| Nafion-NdZr (1%)/[P-S]$_2$ | 92.9 | 82.8 | 76.9 | 94.0 | 81.2 | 76.4 | 96.1 | 79.8 | 76.7 | 13 |
| BC−PFSA | | | | 89.2 | 88.5 | 78.9 | | | | 12 |
| SPES (IL-30) | 98.4 | 93.6 | 92.1 | 98.8 | 87.8 | 86.7 | 99.0 | 82.5 | 81.7 | 63 |
| Nafion-(SN@APTES-PWA) −4.5 wt % | 86.4 | 95.0 | 82.0 | 90.8 | 81.5 | 74.0 | | | | 54 |
| CQSPK-6 | 97.3 | 84.1 | 81.8 | 98.7 | 70.8 | 69.8 | | | | 64 |
| 45-C−CNC/PVDFHFP | 94.5 | 95.2 | 90.0 | 97.4 | 91.1 | 88.7 | 98.5 | 86.7 | 85.4 | 65 |
| SPSF/g−C$_3$N$_4$-1 | 95.6 | 93.7 | 89.6 | 98.0 | 89.1 | 87.3 | | | | 22 |
| Im-bPPO | 99.5 | 81.0 | 80.6 | | | | | | | 66 |
| sPP-*b*-PSK | | | | 98.6 | 87.3 | 86.0 | 99.0 | 81.3 | 80.5 | 20 |
| CPBI-70-NMG | | | | 98.0 | 90.7 | 88.9 | 98.8 | 86.4 | 85.3 | 47 |
| CPBI-PEI-20 | | | | 98.3 | 90.6 | 89.1 | 98.8 | 86.6 | 85.5 | 46 |
| HPSf-Im-CD30% | 95.0 | 93.6 | 89.0 | 97.7 | 87.5 | 85.5 | 98.5 | 81.7 | 80.5 | 23 |
| B-PBI | | | | 96.1 | 88.9 | 85.4 | 97.4 | 84.9 | 82.7 | 35 |
| NP-15 | 99.1 | 92.6 | 91.8 | 99.2 | 87.4 | 86.7 | 99.7 | 81.6 | 81.3 | 36 |
| PVDF/SiO$_2$−SO$_3$H-42 | 78.3 | 83.8 | 65.6 | 88.5 | 70.8 | 62.6 | | | | 67 |
| NaCl-5 M | 98.6 | 94.5 | 93.2 | 99.4 | 87.4 | 86.9 | 99.5 | 83.1 | 82.7 | 68 |

The introduction of SZW as redox-active ion barriers increases the resistance of vanadium-ion transport. Meanwhile, the sulfonic groups of SZW could interact with the imidazole-hydroxyl-quaternary ammonium groups of PG112 to form the hydrogen-bond network, which is of benefit to improve the CE of membrane. After introducing SZW, the VFBs assembled with the PG112-SZW$_x$-*X* membrane present an improvement in CE. Meanwhile, the PG112-SZW$_x$-1 membrane showed similar CE, which is in agreement with the measurement results of $VO^{2+}$ permeabilities. The PG112-SZW$_{0.4}$-1 membrane shows a higher CE of 97.5−99.2% than the PG112 (96.2−98.6%), PG93 (96.1−98.4%), and Nafion 212 (77.9−92.8%) membranes at 40−120 mA cm$^{-2}$, which is mainly caused by lower $VO^{2+}$ permeability (Figure 6a). A slight decrease in VE happens due to the introduction of SZW. The VEs of PG112-SZW$_{0.4}$-1 (95.5−86.8%) are still higher than those of PG93 (94.8−86.1%) at 40−120 mA cm$^{-2}$ due to the effect of the strong acidic ability of SZW (Figure 6b). The sulfonic groups of SZW could promote the proton transport, and the formed hydrogen-bond network constructs continuous ion-transport channels for high proton conductivity. As an effective index, energy efficiency (EE) is used to assess cell


https://dx.doi.org/10.1021/acssuschemeng.0c05359
ACS Sustainable Chem. Eng. XXXX, XXX, XXX−XXX

performance, which is affected by CE and VE, simultaneously. The PG112-SZW$_{0.4}$-1 membrane used in the cell shows an optimistic EE of ~90% at 80 mA cm$^{-2}$, being nearly 10% higher than that with Nafion 212 (80.4%) and approximate to the value of PG112 (90.2%) membranes (Figure 6c). At the same SR and WU, the EE of PG112-SZW$_{0.4}$-1 (93.1−86.0%) is higher than that of PG93 (91.1−84.7%). It is because of the synergistic effect of redox-active ion barriers and proton conductors of SZW. So far, PG112-SZW$_{0.4}$-1 shows impressive EEs among the membranes reported in recent years, according to our knowledge (Table 2).

The self-discharges of samples were also tested (Figure 7). The PG112-SZW$_{0.4}$-1 membrane has a long self-discharge duration time of 231 h, which is 6.6 times that with Nafion 212 (35 h) and 2.6 times that with PG112 (88 h). This indicates that the PG112-SZW$_{0.4}$-1 membrane has excellent resistance of vanadium permeation, which agrees with the result of $VO^{2+}$ permeation measurement. The favorable performance indicates that the PG112-SZW*x*-X membrane is a good candidate for use in the VFB system.

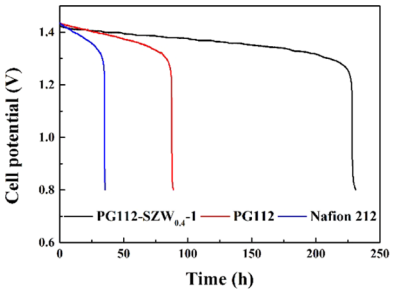


**Figure 7.** Self-discharge curves of PG112-SZW$_{0.4}$-1, PG112, and Nafion 212 membranes.

**Cycle Performance.** The charge−discharge cycle performances of the PG112-SZW$_{0.4}$-1 and PG112 membranes were investigated at 120 mA cm$^{-2}$ to evaluate the long-term performance of the membranes (Figure 8). The cell assembled with PG112-SZW$_{0.4}$-1 shows stable efficiencies during 400 cycles (Figure 8a). After 400 cycles, the CE is still nearly 99.0%, which is higher than that of PG112 (98.0%) ascribing to the low $VO^{2+}$ crossover and good stability of the membrane. The discharge capacity retention of PG112-SZW$_{0.4}$-1 (86.7%) is almost 10% higher than that of PG112 (77.8%) and nearly 40% more than that with Nafion 212 (50.5%) after 50 cycles. The charge capacities of PG112-SZW$_{0.4}$-1, PG112, and Nafion 212 after 50 cycles decreased by 13.2, 22.1, and 49.5%, respectively. The lower capacity loss of PG112-SZW$_{0.4}$-1 can be attributed to the low $VO^{2+}$ crossover (Figure 8b). The fluctuation of discharge capacity during cycling is possibly caused by the temperature fluctuation in the VFB operation. The stable cycle efficiencies and high capacity retention of the PG112-SZW$_{0.4}$-1 membranes ensure the stable long-term operation of VFB.

## CONCLUSIONS

The SZW nanofillers were prepared and applied to break through the trade-off between ion selectivity and ion conductivity of the PG112 membrane in a vanadium flow battery. The morphology, vanadium-ion penetration, and battery performance of prepared membranes were measured and discussed in detail. The addition of the SZW nanofillers lowered the vanadium-ion permeation and also promoted proton transport. The vanadium-ion permeability (7.86 × 10$^{-10}$ cm$^2$ s$^{-1}$) is much lower than those of PG112 (3.93 × 10$^{-9}$ cm$^2$ s$^{-1}$) and Nafion 212 (7.76 × 10$^{-8}$ cm$^2$ s$^{-1}$). Meanwhile, the proton conductivity of the PG112-SZW$_x$-*X* membrane is comparable to that of PG112. Thus, the cell with the PG112-SZW$_{0.4}$-1 membrane exhibits a much higher CE of 97.5−99.1% than PG112 (96.2−98.6%) and Nafion 212 (CE: 78.0−92.8%) at 40−120 mA cm$^{-2}$. Low capacity fading and no obvious performance change during cycle test demonstrate the high chemical stability of the membrane. Moreover, the self-discharge duration time (231 h) is much longer than those of PG112 (88 h) and Nafion 212 (35 h).

## AUTHOR INFORMATION

### Corresponding Authors

**Xiaoming Yan** − *State Key Laboratory of Fine Chemicals, R&D Center of Membrane Science and Technology, School of Chemical Engineering, and Panjin Institute of Industrial Technology, Dalian University of Technology, Dalian 116023, China;* orcid.org/0000-0002-5263-9952; Email: yanxiaoming@dlut.edu.cn

**Baigang An** − *School of Chemical Engineering, University of Science and Technology Liaoning, Anshan 114051, China;* Email: bgan@ustl.edu.cn

**Gaohong He** − *State Key Laboratory of Fine Chemicals, R&D Center of Membrane Science and Technology, School of Chemical Engineering, and Panjin Institute of Industrial Technology, Dalian University of Technology, Dalian 116023, China;* orcid.org/0000-0002-6674-8279; Email: hgaohong@dlut.edu.cn

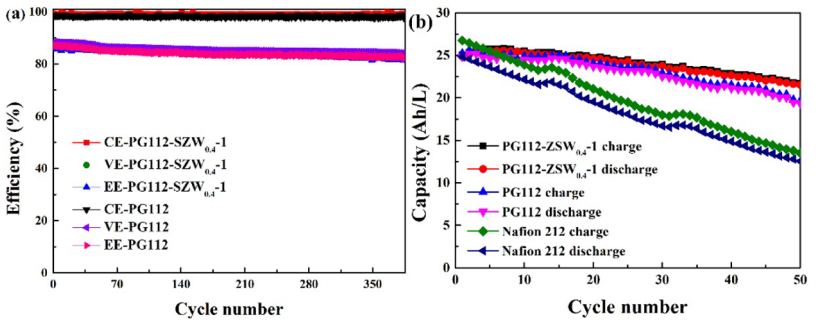


**Figure 8.** (a) Cycling performance of PG112-SZW$_{0.4}$-1 and PG112 membranes at 120 mA cm$^{-2}$; (b) capacity decay of PG112-SZW$_{0.4}$-1, PG112, and Nafion 212 membrane at 120 mA cm$^{-2}$.



https://dx.doi.org/10.1021/acssuschemeng.0c05359
ACS Sustainable Chem. Eng. XXXX, XXX, XXX−XXX

### Authors

**Lei Hu** − *State Key Laboratory of Fine Chemicals, R&D Center of Membrane Science and Technology and School of Chemical Engineering, Dalian University of Technology, Dalian 116023, China*

**Yue Du** − *State Key Laboratory of Fine Chemicals, R&D Center of Membrane Science and Technology, Dalian University of Technology, Dalian 116023, China; School of Chemical Engineering, University of Science and Technology Liaoning, Anshan 114051, China*

**Li Gao** − *State Key Laboratory of Fine Chemicals, R&D Center of Membrane Science and Technology, Dalian University of Technology, Dalian 116023, China*

**Mengting Di** − *State Key Laboratory of Fine Chemicals, R&D Center of Membrane Science and Technology, Dalian University of Technology, Dalian 116023, China*

**Ning Zhang** − *State Key Laboratory of Fine Chemicals, R&D Center of Membrane Science and Technology and School of Chemical Engineering, Dalian University of Technology, Dalian 116023, China;* orcid.org/0000-0003-2893-5505

**Yu Pan** − *State Key Laboratory of Fine Chemicals, R&D Center of Membrane Science and Technology and School of Chemical Engineering, Dalian University of Technology, Dalian 116023, China*

Complete contact information is available at: https://pubs.acs.org/10.1021/acssuschemeng.0c05359


### Author Contributions

⊥L.H. and Y.D. contributed equally to this work.

### Notes

The authors declare no competing financial interest.

## ■ ACKNOWLEDGMENTS

This work was supported by the National Natural Science Foundation of China (grant nos. U1808209, U1663223, 21527812, and 21706023) and Science Fund for Creative Research Groups of the National Natural Science Foundation of China (22021005).

## ■ REFERENCES


(1) Zhang, C.; Zhang, L.; Ding, Y.; Peng, S.; Guo, X.; Zhao, Y.; He, G.; Yu, G. Progress and prospects of next-generation redox flow batteries. *Energy Storage Mater.* **2018**, *15*, 324−350.

(2) Marichelvam, T.; Manzoor Bhat, Z.; Thimmappa, R.; Devendrachari, M. C.; Kottaichamy, A. R.; Naranammalpuram Sundaram, V. N.; Thotiyl, M. O. Hydrogen Fuel Exhaling Zn−Ferricyanide Redox Flow Battery. *ACS Sustainable Chem. Eng.* **2019**, *7*, 16241−16246.

(3) Ulaganathan, M.; Suresh, S.; Mariyappan, K.; Periasamy, P.; Pitchai, R. New Zinc−Vanadium (Zn−V) Hybrid Redox Flow Battery: High-Voltage and Energy-Efficient Advanced Energy Storage System. *ACS Sustainable Chem. Eng.* **2019**, *7*, 6053−6060.

(4) Ding, Y.; Zhang, C.; Zhang, L.; Zhou, Y.; Yu, G. Molecular engineering of organic electroactive materials for redox flow batteries. *Chem. Soc. Rev.* **2018**, *47*, 69−103.

(5) Ding, Y.; Zhang, C.; Zhang, L.; Zhou, Y.; Yu, G. Pathways to Widespread Applications: Development of Redox Flow Batteries Based on New Chemistries. *Chem* **2019**, *5*, 1964−1987.

(6) Zhang, L.; Ding, Y.; Zhang, C.; Zhou, Y.; Zhou, X.; Liu, Z.; Yu, G. Enabling Graphene-Oxide-Based Membranes for Large-Scale Energy Storage by Controlling Hydrophilic Microstructures. *Chem* **2018**, *4*, 1035−1046.

(7) Zhang, L.; Zhang, C.; Ding, Y.; Ramirez-Meyers, K.; Yu, G. A Low-Cost and High-Energy Hybrid Iron-Aluminum Liquid Battery Achieved by Deep Eutectic Solvents. *Joule* **2017**, *1*, 623−633.

(8) Chae, I. S.; Luo, T.; Moon, G. H.; Ogieglo, W.; Kang, Y. S.; Wessling, M. Ultra-High Proton/Vanadium Selectivity for Hydrophobic Polymer Membranes with Intrinsic Nanopores for Redox Flow Battery. *Adv. Energy Mater.* **2016**, *6*, No. 1600517.

(9) Zhou, X. L.; Zhao, T. S.; An, L.; Zeng, Y. K.; Wei, L. Critical transport issues for improving the performance of aqueous redox flow batteries. *J. Power Sources* **2017**, *339*, 1−12.

(10) Li, N.; Guiver, M. D. Ion Transport by Nanochannels in Ion-Containing Aromatic Copolymers. *Macromolecules* **2014**, *47*, 2175−2198.

(11) Jiang, B.; Wu, L.; Yu, L.; Qiu, X.; Xi, J. A comparative study of Nafion series membranes for vanadium redox flow batteries. *J. Membr. Sci.* **2016**, *510*, 18−26.

(12) Palanisamy, G.; Sadhasivam, T.; Park, W.-S.; Bae, S. T.; Roh, S.-H.; Jung, H.-Y. Tuning the Ion Selectivity and Chemical Stability of a Biocellulose Membrane by PFSA Ionomer Reinforcement for Vanadium Redox Flow Battery Applications. *ACS Sustainable Chem. Eng.* **2020**, *8*, 2040−2051.

(13) Hossain, S. I.; Aziz, M. A.; Shanmugam, S. Ultrahigh Ion-Selective and Durable Nafion-NdZr Composite Layer Membranes for All-Vanadium Redox Flow Batteries. *ACS Sustainable Chem. Eng.* **2020**, *8*, 1998−2007.

(14) Xi, J.; Jiang, B.; Yu, L.; Liu, L. Membrane evaluation for vanadium flow batteries in a temperature range of −20−50 °C. *J. Membr. Sci.* **2017**, *522*, 45−55.

(15) Zhang, D.; Wang, Q.; Peng, S.; Yan, X.; Wu, X.; He, G. An interface-strengthened cross-linked graphene oxide/Nafion212 composite membrane for vanadium flow batteries. *J. Membr. Sci.* **2019**, *587*, No. 117189.

(16) Gu, S.; Xu, B.; Yan, Y. Electrochemical energy engineering: a new frontier of chemical engineering innovation. *Annu. Rev. Chem. Biomol. Eng.* **2014**, *5*, 429−454.

(17) Li, X.; Zhang, H.; Mai, Z.; Zhang, H.; Vankelecom, I. Ion exchange membranes for vanadium redox flow battery (VRB) applications. *Energy Environ. Sci.* **2011**, *4*, 1147−1160.

(18) Tang, A.; Bao, J.; Skyllas-Kazacos, M. Studies on pressure losses and flow rate optimization in vanadium redox flow battery. *J. Power Sources* **2014**, *248*, 154−162.

(19) He, G.; Li, Z.; Zhao, J.; Wang, S.; Wu, H.; Guiver, M. D.; Jiang, Z. Nanostructured Ion-Exchange Membranes for Fuel Cells: Recent Advances and Perspectives. *Adv. Mater.* **2015**, *27*, 5280−5295.

(20) Hong, S. H.; Cha, M. S.; Hong, S.-K.; Oh, S.-G.; Lee, J. Y. Structural Effect of the Hydrophobic Block on the Chemical Stability of Ion-Conducting Multiblock Copolymers for Flow Battery. *ACS Sustainable Chem. Eng.* **2019**, *7*, 17088−17099.

(21) Choi, S. W.; Kim, T. H.; Jo, S. W.; Lee, J. Y.; Cha, S. H.; Hong, Y. T. Hydrocarbon membranes with high selectivity and enhanced stability for vanadium redox flow battery applications: Comparative study with sulfonated poly(ether sulfone)s and sulfonated poly(thioether ether sulfone)s. *Electrochim. Acta* **2018**, *259*, 427−439.

(22) Liu, B.; Zhang, Y.; Jiang, Y.; Qian, P.; Shi, H. High performance acid-base composite membranes from sulfonated polysulfone containing graphitic carbon nitride nanosheets for vanadium redox flow battery. *J. Membr. Sci.* **2019**, *591*, No. 117332.

(23) Ma, Y.; Li, L.; Ma, L.; Qaisrani, N. A.; Gong, S.; Li, P.; Zhang, F.; He, G. Cyclodextrin templated nanoporous anion exchange membrane for vanadium flow battery application. *J. Membr. Sci.* **2019**, *586*, 98−105.

(24) Huang, T.; He, G.; Xue, J.; Otoo, O.; He, X.; Jiang, H.; Zhang, J.; Yin, Y.; Jiang, Z.; Douglin, J. C.; Dekel, D. R.; Guiver, M. D. Self-crosslinked blend alkaline anion exchange membranes with bi-continuous phase separated morphology to enhance ion conductivity. *J. Membr. Sci.* **2020**, *597*, No. 117769.

(25) Yu, L.; Yu, L.; Wang, L.; Wang, L.; Qiu, X.; Xi, J. Bilayer Designed Hydrocarbon Membranes for All-Climate Vanadium Flow

Batteries To Shield Catholyte Degradation and Mitigate Electrolyte Crossover. *ACS Appl. Mater. Interfaces* **2019**, *11*, 13285−13294.
(26) Mu, D.; Yu, L.; Liu, L.; Xi, J. Rice Paper Reinforced Sulfonated Poly(ether ether ketone) as Low-Cost Membrane for Vanadium Flow Batteries. *ACS Sustainable Chem. Eng.* **2017**, *5*, 2437−2444.
(27) Zheng, L.; Wang, H.; Niu, R.; Zhang, Y.; Shi, H. Sulfonated poly(ether ether ketone)/sulfonated graphene oxide hybrid membrane for vanadium redox flow battery. *Electrochim. Acta* **2018**, *282*, 437−447.
(28) Zhang, Y.; Wang, H.; Liu, B.; Shi, J.; Zhang, J.; Shi, H. An ultra-high ion selective hybrid proton exchange membrane incorporated with zwitterion-decorated graphene oxide for vanadium redox flow batteries. *J. Mater. Chem. A* **2019**, *7*, 12669−12680.
(29) Lai, Y.; Wan, L.; Wang, B. PVDF/Graphene Composite Nanoporous Membranes for Vanadium Flow Batteries. *Membranes* **2019**, *9*, No. 89.
(30) Xue, R.; Jiang, F.; Wang, F.; Zhou, X. Towards cost-effective proton-exchange membranes for redox flow batteries: A facile and innovative method. *J. Power Sources* **2020**, *449*, No. 227475.
(31) Yu, L.; Wang, L.; Yu, L.; Mu, D.; Wang, L.; Xi, J. Aliphatic/aromatic sulfonated polyimide membranes with cross-linked structures for vanadium flow batteries. *J. Membr. Sci.* **2019**, *572*, 119−127.
(32) Yang, P.; Long, J.; Xuan, S.; Wang, Y.; Zhang, Y.; Li, J.; Zhang, H. Branched sulfonated polyimide membrane with ionic cross-linking for vanadium redox flow battery application. *J. Power Sources* **2019**, *438*, No. 226993.
(33) Long, J.; Yang, H. Y.; Wang, Y. L.; Xu, W. J.; Liu, J.; Luo, H.; Li, J. C.; Zhang, Y. P.; Zhang, H. P. Branched Sulfonated Polyimide/Sulfonated Methylcellulose Composite Membranes with Remarkable Proton Conductivity and Selectivity for Vanadium Redox Flow Batteries. *ChemElectroChem* **2020**, *7*, 937−945.
(34) Luo, T.; Dreusicke, B.; Wessling, M. Tuning the ion selectivity of porous poly(2,5-benzimidazole) membranes by phase separation for all vanadium redox flow batteries. *J. Membr. Sci.* **2018**, *556*, 164−177.
(35) Chen, D.; Qi, H.; Sun, T.; Yan, C.; He, Y.; Kang, C.; Yuan, Z.; Li, X. Polybenzimidazole membrane with dual proton transport channels for vanadium flow battery applications. *J. Membr. Sci.* **2019**, *586*, 202−210.
(36) Geng, K.; Li, Y.; Xing, Y.; Wang, L.; Li, N. A novel polybenzimidazole membrane containing bulky naphthalene group for vanadium flow battery. *J. Membr. Sci.* **2019**, *586*, 231−239.
(37) Jiang, B.; Hu, L.; Yan, X.; Sun, J.; Gao, L.; Dai, Y.; Ruan, X.; He, G. A new long-side-chain sulfonated poly(2,6-dimethyl-1,4-phenylene oxide) (PPO) /polybenzimidazole (PBI) amphoteric membrane for vanadium redox flow battery. *Chinese. J. Chem. Eng.* **2020**, *28*, 1918−1924.
(38) Zhou, X. L.; Zhao, T. S.; An, L.; Wei, L.; Zhang, C. The use of polybenzimidazole membranes in vanadium redox flow batteries leading to increased coulombic efficiency and cycling performance. *Electrochim. Acta* **2015**, *153*, 492−498.
(39) Li, X.; Ma, H.; Wang, P.; Liu, Z.; Peng, J.; Hu, W.; Jiang, Z.; Liu, B.; Guiver, M. D. Highly Conductive and Mechanically Stable Imidazole-Rich Cross-Linked Networks for High-Temperature Proton Exchange Membrane Fuel Cells. *Chem. Mater.* **2020**, *32*, 1182−1191.
(40) Li, X.; Ma, H.; Shen, Y.; Hu, W.; Jiang, Z.; Liu, B.; Guiver, M. D. Dimensionally-stable phosphoric acid−doped polybenzimidazoles for high-temperature proton exchange membrane fuel cells. *J. Power Sources* **2016**, *336*, 391−400.
(41) Jiang, B.; Hu, L.; Yan, X.; Sun, J.; Gao, L.; Dai, Y.; Ruan, X.; He, G. A new long-side-chain sulfonated poly(2,6-dimethyl-1,4-phenylene oxide)/polybenzimidazole amphoteric membrane for vanadium redox flow battery. *Chin. J. Chem. Eng.* **2020**, *28*, 1918−1924.
(42) Noh, C.; Jung, M.; Henkensmeier, D.; Nam, S. W.; Kwon, Y. Vanadium Redox Flow Batteries Using meta-Polybenzimidazole-Based Membranes of Different Thicknesses. *ACS Appl. Mater. Interfaces* **2017**, *9*, 36799−36809.
(43) Yuan, Z.; Duan, Y.; Zhang, H.; Li, X.; Zhang, H.; Vankelecom, I. Advanced porous membranes with ultra-high selectivity and stability for vanadium flow batteries. *Energy Environ. Sci.* **2016**, *9*, 441−447.
(44) Qiao, L.; Zhang, H. M.; Lu, W. J.; Dai, Q.; Li, X. F. Advanced Porous Membranes with Tunable Morphology Regulated by Ionic Strength of Nonsolvent for Flow Battery. *ACS Appl. Mater. Interfaces* **2019**, *11*, 24107−24113.
(45) Lu, W.; Yuan, Z.; Zhao, Y.; Qiao, L.; Zhang, H.; Li, X. Advanced porous PBI membranes with tunable performance induced by the polymer-solvent interaction for flow battery application. *Energy Storage Mater.* **2018**, *10*, 40−47.
(46) Hu, L.; Gao, L.; Zhang, C. K.; Yan, X. M.; Jiang, X. B.; Zheng, W. J.; Ruan, X. H.; Wu, X. M.; Yu, G. H.; He, G. H. "Fishnet-like" ion-selective nanochannels in advanced membranes for flow batteries. *J. Mater. Chem. A* **2019**, *7*, 21112−21119.
(47) Hu, L.; Gao, L.; Yan, X. M.; Zheng, W. J.; Dai, Y.; Hao, C.; Wu, X. M.; He, G. H. Proton delivery through a dynamic 3D H-bond network constructed from dense hydroxyls for advanced ion-selective membranes. *J. Mater. Chem. A* **2019**, *7*, 15137−15144.
(48) Peng, S. S.; Wu, X. M.; Yan, X. M.; Gao, L.; Zhu, Y. Z.; Zhang, D. S.; Li, J.; Wang, Q.; He, G. H. Polybenzimidazole membranes with nanophase-separated structure induced by non-ionic hydrophilic side chains for vanadium flow batteries. *J. Mater. Chem. A* **2018**, *6*, 3895−3905.
(49) Ding, L.; Song, X.; Wang, L.; Zhao, Z. Enhancing proton conductivity of polybenzimidazole membranes by introducing sulfonate for vanadium redox flow batteries applications. *J. Membr. Sci.* **2019**, *578*, 126−135.
(50) Du, Y.; Gao, L.; Hu, L.; Di, M.; Yan, X.; An, B.; He, G. The synergistic effect of protonated imidazole-hydroxyl-quaternary ammonium on improving performances of anion exchange membrane assembled flow batteries. *J. Membr. Sci.* **2020**, *603*, No. 118011.
(51) Shanmugam, S.; Viswanathan, B.; Varadarajan, T. K. Synthesis and characterization of silicotungstic acid based organic−inorganic nanocomposite membrane. *J. Membr. Sci.* **2006**, *275*, 105−109.
(52) Liu, S.; Sang, X.; Wang, L.; Zhang, J.; Song, J.; Han, B. Incorporation of metal-organic framework in polymer membrane enhances vanadium flow battery performance. *Electrochim. Acta* **2017**, *257*, 243−249.
(53) Dai, W.; Shen, Y.; Li, Z.; Yu, L.; Xi, J.; Qiu, X. SPEEK/Graphene oxide nanocomposite membranes with superior cyclability for highly efficient vanadium redox flow battery. *J. Mater. Chem. A* **2014**, *2*, 12423−12432.
(54) Yang, X.-B.; Zhao, L.; Goh, K.; Sui, X.-L.; Meng, L.-H.; Wang, Z.-B. A phosphotungstic acid coupled silica-Nafion composite membrane with significantly enhanced ion selectivity for vanadium redox flow battery. *J. Energy Chem.* **2020**, *41*, 177−184.
(55) Stoyanov, E. S.; Stoyanova, I. V. Features of Protonation of the Simplest Weakly Basic Molecules, SO2, CO, N2 O, CO2, and Others by Solid Carborane Superacids. *Angew. Chem., Int. Ed.* **2018**, *57*, 4516−4520.
(56) Wang, J.; Zhang, Y.; Wu, H.; Xiao, L.; Jiang, Z. Fabrication and performances of solid superacid embedded chitosan hybrid membranes for direct methanol fuel cell. *J. Power Sources* **2010**, *195*, 2526−2533.
(57) Huang, Y. Y.; Zhao, B. Y.; Xie, Y. C. Modification of sulfated zirconia by tungsten oxide: Acidity enhancement and structural characterization. *Appl. Catal., A* **1998**, *171*, 75−83.
(58) Fan, M.; Si, Z.; Sun, W.; Zhang, P. Sulfonated ZrO2-TiO2 nanorods as efficient solid acid catalysts for heterogeneous esterification of palmitic acid. *Fuel* **2019**, *252*, 254−261.
(59) Reddy, B. M.; Reddy, G. K.; Rao, K. N.; Katta, L. Influence of alumina and titania on the structure and catalytic properties of sulfated zirconia: Beckmann rearrangement. *J. Mol. Catal. A: Chem.* **2009**, *306*, 62−68.
(60) Lewera, A.; Timperman, L.; Roguska, A.; Alonso-Vante, N. Metal−Support Interactions between Nanosized Pt and Metal Oxides ($WO_3$ and $TiO_2$) Studied Using X-ray Photoelectron Spectroscopy. *J. Phys. Chem. C* **2011**, *115*, 20153−20159.


https://dx.doi.org/10.1021/acssuschemeng.0c05359
ACS Sustainable Chem. Eng. XXXX, XXX, XXX−XXX

(61) Wang, T.; Jeon, J. Y.; Han, J.; Kim, J. H.; Bae, C.; Kim, S. Poly(terphenylene) anion exchange membranes with high conductivity and low vanadium permeability for vanadium redox flow batteries (VRFBs). *J. Membr. Sci.* **2020**, *598*, No. 117665.
(62) Teng, X.; Guo, Y.; Liu, D.; Li, G.; Yu, C.; Dai, J. A polydopamine-coated polyamide thin film composite membrane with enhanced selectivity and stability for vanadium redox flow battery. *J. Membr. Sci.* **2020**, *601*, No. 117906.
(63) Zhou, X.; Xue, R.; Zhong, Y.; Zhang, Y.; Jiang, F. Asymmetric porous membranes with ultra-high ion selectivity for vanadium redox flow batteries. *J. Membr. Sci.* **2020**, *595*, No. 117614.
(64) Kumar, S.; Bhushan, M.; Shahi, V. K. Cross-linked amphoteric membrane: Sulphonated poly(ether ether ketone) grafted with 2,4,6-tris(dimethylaminomethyl)phenol using functionalized side chain spacers for vanadium redox flow battery. *J. Power Sources* **2020**, *448*, No. 227358.
(65) Mukhopadhyay, A.; Cheng, Z.; Natan, A.; Ma, Y.; Yang, Y.; Cao, D.; Wang, W.; Zhu, H. Stable and Highly Ion-Selective Membrane Made from Cellulose Nanocrystals for Aqueous Redox Flow Batteries. *Nano Lett.* **2019**, *19*, 8979−8989.
(66) Roh, S.-H.; Lim, M.-H.; Sadhasivam, T.; Jung, H.-Y. Investigation on physico-chemical and electrochemical performance of poly(phenylene oxide)-based anion exchange membrane for vanadium redox flow battery systems. *Electrochim. Acta* **2019**, *325*, No. 134944.
(67) Ling, L.; Xiao, M.; Han, D.; Ren, S.; Wang, S.; Meng, Y. Porous composite membrane of PVDF/Sulfonic silica with high ion selectivity for vanadium redox flow battery. *J. Membr. Sci.* **2019**, *585*, 230−237.
(68) Qiao, L.; Zhang, H.; Lu, W.; Dai, Q.; Li, X. Advanced Porous Membranes with Tunable Morphology Regulated by Ionic Strength of Nonsolvent for Flow Battery. *ACS Appl. Mater. Interfaces* **2019**, *11*, 24107−24113.


https://dx.doi.org/10.1021/acssuschemeng.0c05359
*ACS Sustainable Chem. Eng.* XXXX, XXX, XXX−XXX